

1 **Article title:** The ALBA RNA-binding proteins function redundantly to promote
2 growth and flowering in Arabidopsis.

3 **Running title:** Arabidopsis ALBA proteins

4 Naiqi Wang¹, Meachery Jalajakumari¹, Thomas Miller¹, Mohsen Asadi^{1,2}, Anthony A
5 Millar¹.

6 1; Division of Plant Science, Research School of Biology, The Australian National
7 University, Canberra ACT 2601, Australia. 2; Department of Biology, Shahid Bahonar
8 University of Kerman, Kerman 7616914111, Iran

9 **Corresponding Author:** Anthony A Millar; email: tony.millar@anu.edu.au; phone:
10 612-6125-2870. Postal address: Division of Plant Science, Research School of
11 Biology, The Australian National University, Canberra ACT 2601, Australia

12 **Other Author's email addresses:** Naiqi Wang (Nai.Wang@anu.edu.au), Meachery
13 Jalajakumari (Meachery.Jalajakumari@anu.edu.au), Thomas Miller
14 (Thomas.miller@anu.edu.au), Mohsen Asadi (Mohseneasadi@gmail.com).

15 **Date of submission:** September 5th, 2019.

16 **Word count:** 5990

17 **Number of Figures:** 8

18 **Number of Supplementary Figures:** 9

19 **Number of Supplementary Tables:** 1

20 **Highlight:** The RNA-binding ALBA proteins have indistinguishable expression
21 patterns and subcellular localizations in Arabidopsis, acting redundantly to promote
22 growth and flowering via a mechanism that does not strongly affect transcriptome
23 composition.

24

25

26 **Abstract**

27 RNA-binding proteins (RBPs) are critical regulators of gene expression, but have
 28 been poorly studied relative to other classes of gene regulators. Recently,
 29 mRNA-interactome capture identified many Arabidopsis RBPs of unknown function,
 30 including a family of ALBA domain containing proteins. Arabidopsis has three
 31 short-form ALBA homologues (*ALBA1-3*) and three long-form ALBA homologues
 32 (*ALBA4-6*), both of which are conserved throughout the plant kingdom. Despite this
 33 ancient origin, *ALBA-GUS* translational fusions of *ALBA1*, *ALBA2*, *ALBA4*, and
 34 *ALBA5* had indistinguishable expression patterns, all being preferentially expressed in
 35 young, rapidly dividing tissues. Likewise, all four ALBA proteins had
 36 indistinguishable *ALBA-GFP* subcellular localizations in roots, all being preferentially
 37 located to the cytoplasm, consistent with being mRNA-binding. Genetic analysis
 38 demonstrated redundancy within the long-form ALBA family members; in contrast to
 39 single *alba* mutants that all appeared wild-type, a triple *alba456* mutant had slower
 40 rosette growth and a strong delay in flowering-time. RNA-sequencing found most
 41 differentially expressed genes in *alba456* were related to metabolism, not
 42 development. Additionally, changes to the *alba456* transcriptome were subtle,
 43 suggesting ALBA4-6 participates in a process that does not strongly affect
 44 transcriptome composition. Together, our findings demonstrate that ALBA protein
 45 function is highly redundant, and is essential for proper growth and flowering in
 46 Arabidopsis.

47 **Key words:** ALBA proteins, flowering, genetic redundancy, RNA-binding proteins,
 48 Arabidopsis.

49

50 Introduction

51 Post-transcriptional gene regulation is primarily orchestrated via RNA-binding
 52 proteins (RBPs). This class of regulators are known to mediate RNA processing,
 53 modification, localization, stability and translation/expression (Hentze et al., 2018).
 54 Consistent with these fundamental processes, plants contain many hundreds of genes
 55 encoding RBPs, being similar in number to genes encoding transcription factors
 56 (Silverman et al., 2013). However, very little is known about the molecular and
 57 functional roles for the majority of plant RBPs (Cho et al., 2019), with most of our
 58 knowledge being derived from bioinformatic extrapolation from other kingdoms
 59 (Silverman et al., 2013).

60 Recently, the mRNA-binding proteome of Arabidopsis was experimentally
 61 determined using mRNA-interactome capture, a method using UV-cross-linking of
 62 proteins to mRNA, followed by oligo-dT capture of RNA-protein complexes, and
 63 then mass spectrometry to identify and quantitate captured proteins (Reichel et al.,
 64 2016; Zhang et al., 2016; Marondedze et al., 2016). For example, interactome capture
 65 on Arabidopsis etiolated seedlings identified 700 proteins as RBPs, 300 of which were
 66 enriched with high confidence. Eighty percent of these proteins contained a
 67 bioinformatically predicted RNA-binding domain (RBD), and for the majority this
 68 was the first experimental evidence identifying them as RBPs in plants. Amongst
 69 these captured RBPs was a family of proteins that contain an “acetylation lowers
 70 binding affinity” (ALBA) domain (Bell et al., 2002), where five of the six members
 71 were identified as RBPs, four being amongst the most confidently captured proteins
 72 (Reichel et al., 2016).

73 ALBA proteins are highly conserved, being found in all kingdoms of life (Verma et al.,
 74 2014). Structures for ALBA proteins have been experimentally determined in the
 75 archaea (*Sulfolobus solfataricus*), plant (*Arabidopsis thaliana*) and animal (*Homo*
 76 *sapiens*) kingdoms (Wardleworth et al., 2002, Madej et al., 2014, Wu et al., 2018). All
 77 these proteins have similar structures, having dimeric and tetrameric forms which can
 78 interact with DNA and RNA (Tanaka et al., 2012, Guo et al., 2014, da Costa et al.,
 79 2017, Chan et al., 2018), indicating a conserved nucleic acid-binding capacity.
 80 Despite this conserved biochemistry, ALBA proteins in the different kingdoms appear
 81 to have diverse molecular functions. In archaea, ALBA proteins ubiquitously bind to

82 DNA, helping to form highly condensed DNA structures, potentially performing
83 analogous functions as eukaryotic histones (Bell et al., 2002, Wardleworth et al., 2002,
84 Laurens et al., 2012, Jelinska et al., 2005). Archaea ALBA proteins also bind RNA,
85 often interacting specifically with double-strand RNA structures, regulating RNA
86 stability (Guo et al., 2003, Guo et al., 2014, Goyal et al., 2016). In protozoa, most
87 studies of ALBA proteins have focused on their RNA-binding capacity (Subota et al.,
88 2011, Chene et al., 2012). For instance, in the trypanosome *Leishmania*, ALBA
89 proteins can specifically regulate the stability of *AMASTIN* which encodes a
90 transmembrane glycoprotein in a particular development stage, contributing to the
91 control of developmental stage and asexual reproduction (Dupe et al., 2014,
92 Perez-Diaz et al., 2017). In animals, ALBA proteins specifically interact with tRNA.
93 Two ALBA family members, named Rpp20 and Rpp25, are subunits of the
94 Ribonuclease P (RNase P) holoenzyme. Here, an Rpp20/Rpp25 heterodimer
95 specifically bind with pre-tRNA, which is required for the tRNA maturation process
96 performed by the RNase P complex (Hands-Taylor et al., 2010, Reiner et al., 2011).

97 In plants, little is known regarding the ALBA proteins family. For *Arabidopsis*, there
98 are six *ALBA* genes, three of which have a long-form structure that consists of an
99 N-terminal ALBA domain, followed by a C-terminal region that possesses multiple
100 Arginine-Glycine (RGG) repeats (At1g76010, At1g20220, At3g07030). The RGG
101 repeats are RNA recognition motifs that specifically interact with guanine
102 (G)-quadruplexes on RNA (Vasilyev et al., 2015, Ozdilek et al., 2017). The other
103 three ALBA proteins are short-forms, and almost solely consist of the ALBA domain
104 (At1g29250, At2g34160, At3g04620). Such long- and short-form structures are found
105 in other kingdoms, such as the protozoan *Trypanosome brucei* (Subota et al., 2011),
106 suggesting an ancient origin of these different ALBA forms.

107 Currently, information regarding plant ALBA function is only just emerging. Firstly,
108 T-DNA insertional mutations in ALBA long-form genes of either *Arabidopsis*
109 (At1g76010 and At1g20220) or the liverwort *Marchantia polymorpha*, inhibited root
110 hair growth (Honkanen et al., 2016). In another study, the short-form ALBA proteins
111 were found to bind DNA-RNA hybrids *in vitro*, that they localized to both the nucleus
112 and cytoplasm, where they could form either homo- or heterodimers with one another
113 (Yuan et al., 2019). In the nucleus, they were shown to be R-loop readers, binding

114 throughout the genome at locations consistent with the presence of R-loops, where
115 their function is to stabilize the genome (Yuan et al., 2019). Therefore, the short-form
116 ALBA proteins appear to have a clear role in the nucleus related to DNA-binding.
117 This includes a nuclear localized ALBA protein in rice, whose expression is
118 upregulated by water-deficient conditions (Verma et al., 2014). Other rice *ALBA*
119 homologs were also upregulated under stress conditions or treatment with hormones,
120 suggesting a role in stress-adaptation and other physiological processes (Verma et al.,
121 2018). However, plant ALBA proteins must also have an RNA-binding role. They
122 were amongst the most enriched proteins in mRNA-interactome capture (Reichel et al.,
123 2016), and in an RNA-affinity purification experiment, an ALBA protein (At1g76010)
124 was amongst the most enriched proteins (Gosai et al., 2015).

125 Here, we perform an initial molecular and functional analysis of the members of the
126 Arabidopsis ALBA family. We find that despite the short- and long-form ALBA
127 proteins having an ancient origin, they have highly similar expression patterns.
128 Analysis of *alba* T-DNA mutant, shows extensive genetic redundancy exists between
129 the different ALBA proteins, where they appear essential for rosette growth and
130 flowering-time in Arabidopsis. Surprisingly, mutation of an entire ALBA clade did not
131 strongly affect transcriptome composition.

132 **Materials and methods**

133 **Plant material and growth**

134 The wild-type *Arabidopsis thaliana* involved in this project is the Columbia-0 ecotype
135 (Col-0). The *alba4* (SALK_015940), *alba5* (SALK_088909) and *alba6*
136 (SALK_048337) single mutants were obtained from the Arabidopsis Biological
137 Resource Center (ARBC). The seeds were sterilized by chlorine gas for four hours in a
138 sealed desiccator jar and then were germinated on 1/2 Murashige and Skoog (1/2 MS)
139 medium with 7 g/L agar. Growth conditions were either a long-day (16 hours light) or
140 short-day (10 hours light) photoperiod at approximately 100 $\mu\text{mol photons s}^{-1} \text{ m}^{-2}$ at
141 22°C. After approximately 10 days, seedlings were transplanted to Debco® plugger
142 soil with Osmocote® Extra Mini fertilizer (3.5 g/L soil) and Azamax® pesticide (0.75
143 mL/L soil).

144 **RNA extraction, qRT-PCR and RNA sequencing**

145 Samples were processed in 1.5 mL centrifuge tubes being immediately frozen with
146 liquid nitrogen, followed by being finely grounded with plastic pestles. Total RNA
147 was extracted using TRIzol® (1 mL per 500 mg sample). 14 µg RNA was treated with
148 14 µL of RQ1 RNase-Free DNase (Promega) and 1 µL of RNaseOut™ Recombinant
149 RNase Inhibitor (Invitrogen) following the manufacturer's protocol. The RNA was
150 then purified using the Qiagen RNeasy mini kit following the RNeasy column
151 clean-up protocol. The RNA quantity and quality were determined via NanoDrop and
152 agarose gel electrophoresis. cDNA was prepared using SuperScript® III Reverse
153 Transcriptase (Invitrogen), with the addition of RNaseOut™. For qRT-PCR, 0.4 µL 10
154 µM specific primer pairs (mixture of forward and reverse primers) was mixed with 10
155 µL SensiFAST SYBR (Bioline) mastermix and 9.6 µL of cDNA. All the qRT-PCR
156 reactions were performed in three technical replicates, carried out by a QIAGEN
157 Rotor-Gene-Q real-time PCR machine. The comparative quantity of each sample was
158 analyzed with the Rotor-Gene 6000 series software (QIAGEN). The *CYCLOPHILIN*
159 (*At2g29960*) was used to normalize the mRNA quantities.

160 For RNA-seq, total RNA was extracted from three biological replicates of
161 seven-day-old *alba456* and *Col-0* seedlings. Quality of purified RNA samples was
162 determined by Nanodrop, agarose gel electrophoresis and via LabChIP GXII
163 (PerkinElmer) analysis. Library preparation, RNA sequencing, differentially
164 expressed gene analysis and GO enrichment analysis were all performed by Beijing
165 Genomics Institute (BGI), Hong Kong.

166 **Generation of *ALBA:GUS* or *ALBA:GFP* transgenic *Arabidopsis***

167 Primers were designed amplify genomic fragments of ALBA genes encompassing 5'
168 regions, exons/introns to the end of the gene except the stop codon (Table S2). *attB1*
169 and *attB2* sites were included to enable Gateway cloning. The amplification of ALBA
170 genome sequences was carried out with high-fidelity KOD Hot Start DNA
171 Polymerase (Merck Millipore), according to the manufacturer's protocol. Amplicons
172 of correct size were gel purified with Wizard® SV Gel and PCR Clean-Up System
173 (Promega). Amplicons were cloned into *pDONR/Zeo* (Invitrogen) using the Gateway
174 BP Clonase II enzyme mix (Invitrogen), and transformed into *Escherichia coli*
175 α-select chemically competent cells (Bioline) via heat shock. Plasmids were screen
176 via restriction enzyme analysis and then entire insert was sequenced to ensure no

177 amplification errors. All correct *ALBA* sequences were then subcloned into *pMDC111*
178 and *pMDC164* destination vectors (Curtis and Grossniklaus, 2003) separately to
179 generate expression clones using Gateway LR Clonase II enzyme mix (Invitrogen).
180 The *ALBA*-reporter gene junction was verified via DNA sequencing to ensure the
181 fusion gene was in frame. Expression clones were transformed into *Agrobacterium*
182 *tumefaciens* *GV3101* via electroporation and were selected on LB plates containing
183 Rifamycin (50 µg/mL), Gentamicin (25 µg/mL) and Kanamycin (50 µg/mL) and
184 verified by restriction enzyme digestion and used to transform *Arabidopsis* by
185 standard procedures (Clough and Bent, 1998).

186 **GUS staining**

187 The *ALBA-GUS* transgenic *Arabidopsis* seedlings were fixed with cold 90% acetone
188 for 20 minutes and washed three times with 1X PBS. Then they were vacuum
189 infiltrated in X-Gluc solution [1 mg/mL X-Gluc, 1.66% N,N-dimethyl formamide, 2%
190 ferricyanide (5 mM), 2% ferrocyanide (5 mM), 50% Triton X-100 (0.3%), 4%
191 phosphate buffer (0.5 M), 20% methanol], and incubation at 37°C for 2 hours.
192 Seedlings were then de-stained with 70%-80% ethanol and observed and
193 photographed using a Leica M205C fluorescence microscope.

194 **DAPI staining and visualization of GFP**

195 The *ALBA-GFP* transgenic *Arabidopsis* seedlings were placed on slides, fixed in 0.1%
196 triton X-100 (diluted in PBS) for 15 minutes and then washed three times in 1X PBS.
197 Samples were then stained by 1 µL/mL DAPI (4',6-diamidino-2-phenylindole) stored
198 in the dark until confocal microscopy. Visualization and photography were performed
199 using the Zeiss LSM780 or the Leica SP8 confocal microscope. The GFP was excited
200 under 488 nm laser and was observed under 500 ~ 530 nm spectral detection. The
201 DAPI was excited with 405 nm laser and was observed under 460 spectral detection

202 **Genotyping and phenotyping of T-DNA *Arabidopsis* mutants**

203 DNA was extracted from *Arabidopsis* young rosette leaves (Edwards et al., 1991), and
204 the presence of T-DNA alleles or wild-type alleles was tested via PCR using
205 gene-specific and the LBb1.3 primers (Table S3) using the GoTaq® Hot Start
206 Polymerase (Promega). The program was: denaturation at 95°C for 2 minutes;

207 followed by 95°C for 45 seconds, 55°C for 45 seconds and 72°C for 90 seconds for
208 35 cycles; then the extension 72°C for 5 minutes. The PCR products were analyzed on
209 1% agarose gel and the position of T-DNA insertions were verified via sequencing the
210 DNA amplicons.

211 For phenotyping, mutant and wild-type (Col-0) plants were planted side-by-side on
212 the same tray and seed was collected from these plants. These seeds were then sown
213 on 0.5X MS-agar plates. For determining the germination rate, seeds were assessed
214 every 15 hours after being placed in the growth chamber, and germination was
215 defined as radicle protrusion from the seed. At 8-9 days old, seedling were then were
216 transplanted side-by-side into trays of soil comprising of 30 individuals (5 columns X
217 6 rows). The rosette area was measured via a LemnaTec Scanalyzer every two days at
218 11 am to 13 pm to ensure the measurements were consistent over the growth period.
219 No further measurements were made once the rosette overlapped with each other on
220 the trays. The flowering-time, the shoot growth and the number of rosette leaves were
221 recorded and counted. The flowering was considered to have occurred when the
222 bolting shoot reached 1 cm (Torti et al., 2012). The rosette leaf were defined as flat
223 leaf with a distinct petiole (Boyes et al., 2001). The counting of rosette leaves was
224 performed every two days at 11 am to 13 pm.

225 **Alignment of ALBA protein sequences**

226 Amino acid sequences were obtained from Phytozome (Goodstein et al., 2012) using
227 keyword searches for ALBA and then the BLAST Tool was used to verify that there
228 were no other ALBA proteins without annotation. The whole protein sequences of all
229 the ALBA proteins of the species of interest were aligned using three multiple
230 sequence alignment programs Clustal Omega
231 (<http://www.ebi.ac.uk/Tools/msa/clustalo/>), MUSCLE
232 (<http://www.ebi.ac.uk/Tools/msa/muscle/>) and COBALT
233 (https://www.ncbi.nlm.nih.gov/tools/cobalt/re_cobalt.cgi). The FASTA format outputs
234 were opened in BioEdit (version 7.2.5;
235 <http://www.mbio.ncsu.edu/BioEdit/bioedit.html>) to visualise and compare. This
236 comparison allowed identification of consistently aligned regions and alternative
237 alignments of problematic areas with closely clustered gaps. The best sequence with
238 the least problematic areas and the alignment of the Alba domain with the least gaps

239 was selected. This was trimmed down to the Alba domain using the NCBI Conserved
240 domain search (<https://www.ncbi.nlm.nih.gov/Structure/cdd/wrpsb.cgi>) to identify the
241 extent of the Alba domain and then the “strip columns containing gaps” function in
242 BioEdit was used. The trimmed alignments were uploaded to IQTREE
243 (<http://iqtree.cibiv.univie.ac.at/>). The job was run at default settings for protein
244 sequences. Trees were visualised using FigTree (v 1.4.3;
245 <http://tree.bio.ed.ac.uk/software/figtree/>).

246 **Statistical and bioinformatics analysis**

247 For qRT-PCR, rosette area size, and rosette leaf number, one-way analysis of variance
248 (ANOVA) was carried out to test whether the traits differed significantly between
249 samples or genotypes. Additionally, before ANOVA analysis, the developmental
250 curves of rosette area size or rosette leaf number were fitted to linear models. After
251 ANOVA, the comparisons between each sample or genotype were performed with
252 Tukey’s honest significant difference (HSD) test. The adjusted p-value (p) < 0.05
253 referred to the statistically significant difference. All analyses and plots were made in
254 R (v3.4.3) and RStudio with the package *ggplot2* v3.1.0 (Wickham, 2016). The linear
255 model was fitted using the *lm* function. The ANOVA and Tuckey’s HSD test were
256 accomplished with the package *multcomp* v1.4-10 (Hothorn et al., 2008). For
257 flowering-time data, the student t-test was performed to compare the different
258 genotypes, using R (v3.4.3) and RStudio with the package *ggpubr* v0.2. Whether
259 segregating populations corresponded to Mendelian ratios was determined by
260 Chi-square test.

261 **Results**

262 **Two distinct clades of ALBA proteins exist throughout the plant kingdom**

263 In Arabidopsis, there are six ALBA genes (Figure 1). Two previous reports have given
264 them different names (Honkanen et al., 2016; Yuan et al., 2019). Although Honkanen
265 et al. (2016) study was first, given the extensive analysis of Yuan et al. (2019), we will
266 follow their ALBA gene nomenclature. There are three shorter-form *ALBA* genes,
267 *ALBA1* (AT1G29250), *ALBA2* (AT2G34160) and *ALBA3* (AT3G04620); and three
268 longer-form *ALBA* genes being *ALBA4* (AT1G76010), *ALBA5* (AT1G20220) and
269 *ALBA6* (AT3G07030) (Figure 1). Phylogenetic finds these shorter and longer forms

270 fall into two distinct clades (data not shown).

271 To investigate whether these two clades exists throughout the plant kingdom, ALBA
272 protein sequences were obtained and analysed from dicotyledonous species
273 (*Arabidopsis thaliana*, *Medicago truncatula*, *Populus trichocarpa* and *Mimulus*
274 *guttatus*), monocotyledonous species (*Oryza sativa* and *Sorghum bicolor*), the basal
275 angiosperm *Amborella trichopoda*, the bryophyte *Physcomitrella patens* (moss) and
276 the single celled green alga *Chlamydomonas reinhardtii*. All protein sequences were
277 obtained from Phytozome, aligned using MUSCLE, trimmed to a 68 amino acid
278 alignment of the ALBA domain and used to generate a phylogenetic tree. It clearly
279 shows that these two clades are found throughout the plant kingdom, which we have
280 named Clade A and Clade B (Figure S1).

281 Clade A proteins are generally shorter with a mean length of approximately 141
282 amino acids, predominantly consist of a single ALBA domain and have a conserved
283 amino acid sequence (NRIQVS) at the start of their ALBA domains. Clade B proteins
284 are generally longer with a mean length of approximately 290 amino acids and most
285 possess a characteristic domain structure of an ALBA domain followed by a more
286 variable region that contains multiple Arginine-Glycine (RGG) repeats (Figure 1).
287 This clade also has a different conserved amino acid sequence (NEIRIT) at the start of
288 the ALBA domain. The tree implies the two different clades arose before the origin
289 and diversification of plants, suggesting they are ancient and fundamental for plant
290 cellular life. Curiously, in the species we examined, there are equal or near-equal
291 numbers of Clade A and Clade B homologues (Figure S1).

292 **Transcript expression analysis of the Arabidopsis ALBA genes**

293 To initiate a molecular characterization of the ALBA gene family in Arabidopsis,
294 ecotype Columbia-0 (Col-0), we used qRT-PCR to quantify the levels of ALBA
295 mRNAs. In general, ALBA1 and ALBA4 have the highest level in Clade A and Clade
296 B respectively (Figure 2). Analysis in different tissues found ALBA1, ALBA2, ALBA5
297 and ALBA6 had similar mRNA levels in vegetative and reproductive parts of the plant
298 ($p>0.05$, ANOVA), whereas ALBA4 exhibited higher mRNA levels in rosettes
299 ($p<0.001$, ANOVA, Tukey's HSD). ALBA3 had higher mRNA levels in flowers
300 ($p<0.001$, ANOVA, Tukey's HSD), suggesting potential tissue specificity (Figure 2A).

301 Analysis of *ALBA* mRNA levels during rosette development found a general trend of
 302 lower mRNA levels as development progressed (Figure 2B). Although this was
 303 clearest for *ALBA4*, for the *ALBA1*, *ALBA2*, *ALBA5* and *ALBA6* genes, the oldest
 304 tissues consistently contained the lowest *ALBA* mRNA levels (Figure 2B). This
 305 suggests these *ALBA* genes are all preferentially transcribed in young tissues. By
 306 contrast, *ALBA3* mRNA levels remained consistently low throughout rosette
 307 development ($p>0.5$, ANOVA) (Figure 2B).

308 **The Arabidopsis ALBA proteins preferentially express in young tissues.**

309 Given that the *ALBA1*, *ALBA2*, *ALBA4* and *ALBA5* have the highest transcript levels,
 310 protein expression patterns were determined for these four genes. To perform this,
 311 these genes were amplified by PCR from Arabidopsis and individually cloned in
 312 frame with the *GUS* reporter gene of the pMDC164 vector (Curtis and Grossniklaus,
 313 2003), to generate *ALBA-GUS* translational fusions (Figure 3A). The isolated *ALBA*
 314 sequences included the 5' intergenic region to the preceding upstream gene and all
 315 coding region introns (Figure S2, Figure 3A). Including these extensive sequences
 316 will help maximize the likelihood that the expression of these *ALBA-GUS* transgenes
 317 reflects that of the endogenous *ALBA* genes. Each *ALBA-GUS* transgene was
 318 individually transformed into Arabidopsis, as well as an empty pMDC164 vector to
 319 act as a negative control.

320 For each *ALBA-GUS* transgene, GUS staining was performed on multiple independent
 321 Arabidopsis transformants that were either 7-, 11-, 15- or 20-days old. In general, all
 322 *ALBA-GUS* transgenes had highly similar expression patterns. From 7- to 20-day old
 323 plants, GUS activity was consistently present in the shoot apex region (SAR) and the
 324 roots, being strongest in the root tips (Figure 3B). Intriguingly, a dynamic expression
 325 pattern of *ALBA-GUS* proteins occurred in leaves. For example, in 7-day-old plants,
 326 strong *ALBA-GUS* expression was found in the cotyledons. However, as the rosette
 327 matured, *ALBA-GUS* expression was lower in mature cotyledons, but was strongly
 328 expressed in newly emerging leaves (Figure 3B). Here, *ALBA-GUS* expression was
 329 highest near the leaf margin (Figure S3A), a region that comprises the marginal
 330 meristem that controls leaf growth after its emergence (Alvarez et al., 2016).
 331 Therefore, consistent with the *ALBA* mRNA levels (Figure 2B), expression appears
 332 strongest in young, rapidly dividing tissues. No staining occurred in the negative

333 control plants.

334 All four *ALBA-GUS* transgenes had highly similar expression pattern in reproductive
335 organs (Figure S3B). In mature flowers, *ALBA1-GUS*, *ALBA2-GUS*, *ALBA4-GUS*
336 and *ALBA5-GUS* expression patterns appeared indistinguishable from one another in
337 stigmas, filaments, pollen and the veins of sepals. In siliques, *ALBA-GUS* expression
338 mainly localized to the top and the base of the silique (Figure S3B). Therefore, all
339 four *ALBA-GUS* expression patterns appeared highly similar, suggesting potential
340 genetic redundancy between these *ALBA* family members.

341 ***ALBA-GFP* fusions predominantly localize to the cytoplasm**

342 To investigate subcellular localization, *ALBA-GFP* translation fusions were generated
343 for *ALBA1*, *ALBA2*, *ALBA4* and *ALBA5* using the identical gene fragments used to
344 generate the *ALBA-GUS* fusions, but using pMDC111 as the destination vector
345 (Curtis and Grossniklaus) (Figure 4A). Transgenic Arabidopsis lines were generated
346 for each construct, and expression was observed via con-focal microscopy. An
347 Arabidopsis *35S-GFP* line was used as a control.

348 In *ALBA-GFP* seedlings, the strongest and clearest GFP fluorescence was observed in
349 root tips, as this tissue had low auto-fluorescence. Here, the expression of all four
350 *ALBA-GFP* transgenes appeared indistinguishable, being expressed the strongest in
351 cells within the meristematic zone, but not in the epidermis nor root cap regions. By
352 contrast, expression of the *35S-GFP* transgene occurred in all root tip cells (Figure
353 4B).

354 Under increased magnification, the subcellular localization of *ALBA-GFP* proteins
355 were determined. Firstly, it was found that *ALBA-GFP* localization appeared mutually
356 exclusive to nuclei, as determined by fluorescence of DAPI staining (Figure 4C). This
357 indicated that the *ALBA-GFP* proteins were predominantly localized in the cytoplasm.
358 In contrast, the GFP proteins in the *35S-GFP* control were localized in both the nuclei
359 and the cytoplasm (Figure 4C). The predominant cytoplasmic subcellular localization
360 of *ALBA-GFP* proteins is consistent with a role of binding mature mRNA, rather than
361 that of DNA. Since chloroplasts also contain DNA, *ALBA-GFP* localization was
362 examined in leaves. It was found that neither *ALBA4-GFP* nor *ALBA5-GFP*
363 overlapped with chlorophyll fluorescence (red signal), indicating they are not

364 localized in chloroplasts (Figure S4). Based on this analysis, ALBA-GFP proteins
365 appear predominantly localized to the cytoplasm.

366 **Generation of an Arabidopsis *alba456* triple mutant**

367 To initiate the functional characterization of the Arabidopsis *ALBA* genes, we chose to
368 focus on *ALBA* genes from Clade B, and investigate whether they are functioning
369 redundantly. To achieve this, the T-DNA insertional mutants *alba4* (SALK_015940),
370 *alba5* (SALK_088909) and *alba6* (SALK_048337) were obtained from the
371 Arabidopsis stock centre (Alonso et al., 2003). The T-DNA insertions were within the
372 coding region for *alba4* and *alba5*, whereas the T-DNA insertion was within the
373 5'-UTR region for *alba6* (Figure 5). All three single mutants appeared phenotypically
374 indistinguishable from wild-type Arabidopsis (data not shown). Given the high amino
375 acid homology of these ALBA proteins, similar expression patterns and identical
376 sub-cellular localizations, these three *ALBA* genes are potentially functionally
377 redundantly with one another. To investigate this, two *alba4-alba5-alba6* (*alba456*)
378 triple mutant plants were generated. An *alba456-1* isolate was isolated from an
379 *ALBA4/alba4-alba5/alba5-alba6/alba6* parent, and an *alba456-2* isolate from an
380 *alba4/alba4-alba5/alba5-ALBA6/alba6* parent. Having two different isolates will
381 reduce the chances of background mutations segregating with the *alba* mutations in
382 both instances. To confirm the loss-of-function of *ALBA* function in *alba456* mutants,
383 qRT-PCR on *alba456-1*, *alba456-2* and Col-0 was performed. The mRNA levels of all
384 three *ALBA* genes have been strongly reduced in the *alba456* mutants, indicating this
385 triple mutant corresponds to a strong loss-of-function *alba* mutant (Figure 5B).

386 ***alba456* exhibited slower rosette growth and delayed flowering-time**

387 To perform a phenotypic comparison between wild-type (Col-0) and *alba456*, seeds
388 of *alba456-1* and *alba456-2* were sown side-by-side with Col-0 on agar plates. No
389 differences were found in the percentages of seeds that germinated or their
390 germination kinetics (Figure S5). Seedlings were transplanted to soil and the rosette
391 growth of each genotype was monitored by determining the rosette area with a
392 Lemnatech Scanalyser every 48 hours and counting the number of rosette leaves.

393 From the 16th day to the 26th day, the rosette area of *alba456* grew significantly slower
394 than Col-0 ($p < 0.001$, linear mixed model, ANOVA, Tukey's HSD) (Figure 6A). From

the 16th day to the 22nd day, *alba456* had a slightly lower number of leaves than *Col-0* ($p>0.05$, linear mixed model, ANOVA) (Figure 6B), that likely contributes to the smaller rosette area. On average, *Col-0* flowered on the 22nd day, whereas *alba456* had an average flowering-time eight days later ($p<0.01$, Student's t-test) (Figure 6C-D). No significant difference in any of the growth traits was detected between *alba456-1* and *alba456-2* ($p>0.05$, Student's t-test). Highly similar rosette growth and flowering-time results were obtained in an independent replication (Figure S6). Additionally, similar reductions to rosette growth and delays to flowering-time were seen under short-day conditions, although the differences were not as strong (Figure S7). These experiments argue *ALBA4*, *ALBA5* and *ALBA6* are required for proper growth and development of Arabidopsis.

The late flower-time phenotype of *alba456* segregated with the *alba* mutations

To determine whether the delayed flowering-time was strictly segregating with the *alba456* mutations, 27 segregating progenies of an *ALBA4/alba4-alba56* and 28 progenies from an *alba45-ALBA6/alba6* mutant were genotyped and scored for their flowering-time (Figure 7). For *ALBA4/alba4-alba56*, five progeny were *alba456* (18.5%), 20 progeny were *ALBA4/alba4-alba56* (74.1%), and two progeny were *ALBA4-alba56* (7.4%). For *alba45-ALBA6/alba6*, one progeny was *alba456* (3.7%), 12 progeny were *alba45-ALBA6/alba6* (42.8%), and 15 progeny were *alba45-ALBA6* (53.6%). Although the segregation did not fit a Mendelian ratio ($p<0.05$, Chi-square test), in both groups the *alba456* progeny had significantly delayed flowering-times ($p<0.01$, analyzed by ANOVA test, Tukey's HSD). By contrast, plants containing *ALBA4* or *ALBA6* alleles had flowering-times more similar to *Col-0* (Figure 7). Thus, this genetically demonstrates that the delayed flowering-time segregated with the *alba* mutations. Furthermore, progeny containing *ALBA4* allele(s) flowered earlier than mutants possessing *ALBA6* allele(s), which suggests *ALBA4* is more predominant than *ALBA6* (Figure 7). This is consistent with the higher mRNA levels of *ALBA4* (Figure 3).

Few mRNAs exhibit high fold-level changes in the *alba456* transcriptome.

Since *ALBA4*, *ALBA5* and *ALBA6* proteins are experimentally demonstrated mRNA-binding proteins (Reichel et al., 2016), to gain insights into their molecular

function, the *alba456* transcriptome was characterized and compared to Col-0. As it was demonstrated that ALBA4 and ALBA5 are strongly and widely expressed in 7-day-old seedlings (Figure 4B), this stage was chosen to perform RNA-seq in a bid to identify the direct effects of the loss-of-function of ALBA4, ALBA5 and ALBA6. RNA from three biological replicates of both Col-0 and *alba456* were prepared and sent to BGI Genomics Co., Ltd for sequencing (BGISEQ-500 platform) and bioinformatic analysis. Over 55 million clean reads were obtained for each of the six samples, for an average of 5.56 Gb bases per sample, with an average mapping ratio of 91.53%, identifying over 23 K gene models.

Firstly, to assess alteration to splicing in *alba456*, differentially spliced genes (DSGs) were identified in the Col-0 and *alba456* transcriptomes. However, only a few genes appeared differentially spliced (Figure S8), indicating that ALBA4-6 were unlikely to play a major or broad role in mRNA processing. Next, differentially expressed genes (DEGs) were identified. Of a total of 23,547 genes, 388 were differentially expressed in *alba456* compared to Col-0 at the two-fold change cutoff, with 173 DEGs being *alba456* upregulated and 215 DEGs being *alba456* downregulated ($P < 0.05$) (Figure 8). The most downregulated genes in *alba456* were *ALBA4*, *ALBA5* and *ALBA6* (Table S1), confirming that *alba456* is a strong loss-of-function *alba* mutant. However, the fold-level changes to the majority of the DEGs was modest; at the five-fold change level, there were only six downregulated genes (three ALBA genes, two hypothetical proteins, and a RAS GTP binding protein), and six upregulated genes (Table S1). The identity of these 12 DEGs was uninformative regarding the understanding the *alba456* phenotype.

The DEGs were functionally annotated by Gene Ontology (GO) enrichment analysis. However, for biological process ontology, there was no significant bias in the annotated terms of the DEGs (Figure S9A). For a more detailed analysis, the identity of the top 50 down- and up-regulated genes in *alba456* was determined (Table S1). Some closely related genes appeared co-regulated. For down-regulated DEGs, this includes two highly related members of the LA RELATED PROTEIN family of RBPs, *LARP6a* and *LARP6b*. Also three members of the ROXY family (also known as *GRX5*, *GRX8* and *GRX11*), are all downregulated. They are involved in cell redox homeostasis, and are all induced by nitrate (Patterson et al., 2016). Conversely, three

members of the *FE-UPTAKE-INDUCING PEPTIDE* family, *IRONMAN 1*, *IRONMAN 2* and *IRONMAN 3*, were upregulated. The expression of these peptide sequences (~ 50 amino acids) is highly responsive to iron deficiency, where they play a role in iron acquisition and homeostasis (Grillet et al., 2018). Similarly, the *RESPONSE TO LOW SULFUR (LSU)* genes, *LSU1* and *LSU3* were both upregulated in *alba456*, and again, both genes encode small proteins (~95 amino acids) (Lewandowska et al., 2010). Other genes related to low sulfur are also induced, including *SULPHUR DEFICIENCY-INDUCED 1*, and *SULFATE TRANSPORTER 1;3*. Therefore, the expression level changes of all these nitrate, iron and sulfur responsive genes suggest *alba456* plants are experiencing nutrient deficiency. Finally, the *ROXY* genes, and many other DEGs have roles in the oxidation-reduction process (Table S1). Supporting a role of ALBA proteins in this process, the *OsALBA1* gene was shown to play a role in tolerance to oxidative stress, via complementation of a yeast mutant (Verma et al., 2014).

Given this, and the absence of any known developmental genes involved in rosette growth or flowering-time, this data suggested the observed phenotypes is related to alterations to metabolism, rather than developmental programs. This is supported by the classification of DEGs based on the Kyoto Encyclopedia of Genes and Genomes (KEGG) database, which demonstrated that most DEGs corresponded to metabolic pathways (Figure S9B). Considering *alba456* exhibits slower rosette growth, whether these alterations to metabolism are direct or indirect effects from lack of ALBA expression is unknown. However, given the small fold-change levels for the majority of DEGs and the modest numbers of DEGs and DSGs, despite ALBA4-6 being RBPs, their loss does not appear to have a strong and widespread impact on the transcriptome.

Discussion

Clade A and Clade B ALBA proteins appear ancient in origin.

In this paper, we carry out molecular and functional characterization of the ALBA family of proteins in Arabidopsis. ALBA proteins are found throughout the plant kingdom and separate into two distinct clades; Clade A, which contained short-form ALBA proteins (consists mainly of a single ALBA domain) and Clade B, long-form ALBA proteins (an N-terminal single ALBA domain with a C-terminal region

490 containing multiple RGG repeats). Given the protozoan *Trypanosoma brucei* has
 491 analogous short-form and long-form ALBA homologues (Subota et al., 2011), these
 492 two ALBA clades must be ancient in origin, and their high conservation implies they
 493 are fundamental for cellular life. Curiously, in many different plant species, Clade A
 494 and Clade B genes are present in a 1:1 ratio. One possible reason for this is that a
 495 short- and long-form ALBA protein specifically dimerize. Although there is evidence
 496 of ALBA proteins dimerizing with one another (Yuan et al., 2019), there is no
 497 evidence of such specific dimerization.

498 **The ALBA genes are preferentially expressed in rapidly dividing tissues.**

499 Despite the apparent ancient origin of the two clades, Clade A (ALBA1 and ALBA2)
 500 and Clade B (ALBA4 and ALBA5) proteins have indistinguishable expression
 501 patterns (Figure 3), suggesting that these proteins are involved in similar
 502 molecular/biological processes. This raised the possibility of functionally redundancy
 503 of not only within an ALBA clade, but between Clade A and Clade B members. The
 504 ALBA genes were expressed highest in young, rapidly dividing tissues. This includes
 505 both root and shoot apex regions. For leaves, the expression of all ALBA:*GUS*
 506 transgenes exhibited a transient pulse of expression, being highly expressed in newly
 507 emerged leaves, but weakly expressed in mature expanded cotyledons/leaves (Figure
 508 3). This leaf expression was highest near the marginal meristem, tissues that promotes
 509 leaf distal growth (Figure 3; Figure S3A) (Alvarez et al., 2016). As all these tissues
 510 are actively dividing, it would be assumed that they are highly metabolically active,
 511 containing high mRNA levels undergoing strong translation which would be required
 512 for cellular growth and expansion.

513 **The ALBA-GFP fusion proteins have similar subcellular localizations.**

514 In addition to these highly similar expression patterns, the subcellular localization of
 515 ALBA1, ALBA2, ALBA4 and ALBA5 appear identical, all being predominantly
 516 located in the cytoplasm when examine in root tips as determined by the expression of
 517 C-terminal fusions of GFP to the ALBA proteins. A cytoplasmic subcellular
 518 localization is consistent with these proteins being mRNA-binding. However, other
 519 reports show conflicting results. One report, using C-terminal ALBA-GFP fusions,
 520 found that ALBA1 and ALBA2 were localized to both the nucleus and cytoplasm

(Yuan et al., 2019). Another study expressed N- and C-terminal GFP fusions with *ALBA1* and *ALBA2* in Arabidopsis, and in agreement with our analysis found *ALBA1* in the cytosol, whereas *ALBA2* was either located to the cytosol (C-terminal) or the cytosol and nucleus (N-terminal) (Palm et al., 2016). In both these studies, the *ALBA*/GFP fusions were transiently expressed with constitutive promoters in mesophyll protoplasts. Similarly, transient assay of the rice OsALBA1 protein in epidermal onion cells was located to both the nucleus and cytoplasm (Verma et al., 2014). By contrast, we stably expressed *ALBA* genes with endogenous promoters and analysed root tips. Such variations in approach could explain the discrepancies between these studies. In other studies using nuclear/cytoplasmic fractionations, *ALBA* proteins were found in the nucleus as well as the cytoplasm (Yuan et al., 2019, Verma et al., 2014).

In multiple kingdoms, *ALBA* proteins have been shown to bind both DNA and RNA, and given that Arabidopsis *ALBA1* and *ALBA2* bind R-loops (Yuan et al., 2019), as well as mRNA (Reichel et al., 2016), it would seem highly likely they are located to both subcellular locations. In other kingdoms, *ALBA* proteins are found in both subcellular locations. Some *ALBA* proteins in protozoa are predominantly localized to the cytoplasm (Mani et al., 2011, Chene et al., 2012), whereas some animal *ALBA* proteins function mainly in the nucleus (Hands-Taylor et al., 2010). In *Leishmania*, some *ALBA* proteins have a dynamic localization, being located predominantly in the cytoplasm or nucleus depending on the developmental stage (Dupe et al., 2015). Therefore, it is possible that plant *ALBA* proteins are also differentially localized, which may depend on expression level, developmental stage and/or environmental factors. Further analyses are required to resolve this.

Perturbed growth and metabolism of the *alba456* mutant.

A delayed flowering-time in the *alba456* triple mutant adds to the number of RBPs that have been implicated in controlling flowering-time (Cho et al., 2019, Steffen et al., 2019). As delayed flowering and reduced rosette growth were not apparent in the corresponding single mutants, this demonstrated functional redundancy between *ALBA4*, *ALBA5* and *ALBA6*. Such an inhibition in growth could be considered consistent with their preferential expression in young, rapidly dividing tissues, where inhibiting the function of these tissues would be expected to negatively impact growth (Figure 2,

3). This is supported by the RNA-seq analysis on the transcriptomes of Col-0 and *alba456*, which found none of the DEGs corresponded to important developmental control genes associated with leaf development or flowering-time (Table S1). This suggests that unlike some RBPs that directly regulate genes in developmental pathways (Steffen et al., 2019), the *alba456* phenotype arises from indirect effects, possibly due to an altered metabolism. Supporting this was the identity of the DEGs and the KEGG enrichment analysis, which found *alba456* DEGs are predominantly related to metabolic pathways, many of which are associated with nutrient deficiency. Therefore, we speculate that perturbation of metabolism slows *alba456* growth, reducing rosette size and delaying flowering-time.

Whether ALBA proteins are directly affecting these DEGs, or whether altered expression of these genes are an indirect consequence of a more general process that is perturbed in *alba456* is unknown. For example, the indirect phenotypic effects were reported for the maize RBP Dek42 that regulates pre-mRNA splicing. The *dek42* mutant predominantly affects starch metabolic processes, but perturbation of this process resulted in seedling lethality (Zuo et al., 2019). The *dek42* mutant caused differential expression to approximately 6% of the transcriptome (Zuo et al., 2019). Similarly, other examples of mutations of RBPs resulted in global changes to the transcriptome. This includes a 14-day old mutant in two RNA recognition motif proteins, RZ-1B and RZ-1C, that had 3,176 DEGs (difference > 1.5-fold, $P < 0.01$) compared to wild-type (Wu et al., 2016). By contrast, much smaller changes to the *alba456* transcriptome were observed; only 1.6% of the *alba456* transcriptome were DEGs at the 2-fold change cutoff (or 0.05% at the 5-fold change cutoff) and there were very few DSGs (Figure S7). This is despite the *alba456* mutant displaying a clear phenotype, and ALBA4-6 being strongly captured RBPs by mRNA-interactome analysis (Reichel et al., 2016). This may suggest that ALBA4-6 may only be regulating a small cohort of mRNAs. Alternatively, the ALBA proteins may be regulating RNA processes that do not directly affect transcriptome composition, such as translational control (Szostak and Gebauer, 2013). The expression of ALBA proteins in rapidly dividing tissues may support the function associated with translation, as one would assume these tissues would have high levels of translational activity. ALBA proteins from other kingdoms regulate translation. In the protozoa *Leishmania*, *Trypanosoma* and *Plasmodium*, the ALBA proteins LiALBA20,

586 *Tc*ALBA30 and *Pf*ALBA1 repress the translation of their target mRNAs (Dupe et al.,
587 2014, Perez-Diaz et al., 2017, Chene et al., 2012).

588 Alternatively, the phenotypes of the *alba456* mutant may not related to their
589 mRNA-binding function, as other ALBA family members have been shown to be
590 associated with R-loops in the nucleus (Yuan et al., 2019), or even possibly playing a
591 role in oxidative stress tolerance (Verma et al., 2014). More work is needed to
592 determine the molecular explanation of the *alba456* phenotype.

593 **Acknowledgments**

594 We would like to thank Daryl Webb (Centre for Advanced Microscopy) for help with
595 con-focal microscopy, Leila Blackman for help with DAPI staining and Teresa
596 Neeman (Biological Data Science Institute) for the biostatistics advice. We thank the
597 Salk Institute Genomic Analysis Laboratory for providing the sequence-indexed
598 Arabidopsis T-DNA insertion mutants. Funding for the SIGnAL indexed insertion
599 mutant collection was provided by the National Science Foundation. Funds for this
600 project were provided by the Research School of Biology, ANU.

601

602 **Figure Legends**

603 **Figure 1. The Arabidopsis ALBA proteins.** AT number, domain structure and
604 amino acid length are shown for each gene.

605 **Figure 2. qRT-PCR transcript profiling of the six Arabidopsis ALBA genes. (A)**
606 mRNA levels in root, rosettes and flowers. **(B)** mRNA levels at different stages of
607 rosette growth. All levels are normalized to *CYCLOPHILIN*. All measurements are
608 the mean of three biological replicates, each of which was determined by three
609 technical replicates ($n=3$). The error bars are the standard deviations.

610 **Figure 3. The expression of ALBA-GUS transgenes during vegetative**
611 **development. (A)** Schematic representation of the *ALBA-GUS* translational fusion for
612 *ALBA1*, *ALBA2*, *ALBA4*, and *ALBA5* in the pMDC163 vector. DNA sequences contain
613 5' intergenic regions, exon and intron region up, but not including the stop codon,
614 were cloned in frame with the *GUS* gene. There will be a “scare” of 28 amino acids
615 between the *ALBA* and *GUS*. LB = left border, RB = right border, *HygroR* =
616 *Hygromycin* resistance gene. The cartoon is not to scale. **(B)** Expression patterns of
617 *ALBA1-GUS*, *ALBA2-GUS*, *ALBA4-GUS*, *ALBA5-GUS* and *pMDC164* transgenic
618 *Arabidopsis* throughout vegetative development (7-, 11-, 15- and 20-day old plants
619 are presented). Each picture is representative of at least three independent primary
620 transformants analysed. The order of the leaf emergence is labeled (“c” denotes
621 cotyledon, “1” denotes the first pair of leaves, “2” denotes the second leaf, etc). The
622 vegetative meristem in the shoot apex region is indicated with black arrows. Scale
623 bars = 2 mm.

624 **Figure 4. The subcellular localization of the ALBA proteins in Arabidopsis roots.**
625 **(A)** Schematic representation of the *ALBA-GFP* translational fusion for *ALBA1*,
626 *ALBA2*, *ALBA4*, and *ALBA5* in the pMDC111 vector. DNA sequences contain 5'
627 intergenic regions, exon and intron region up, but not including the stop codon, were

628 cloned in frame with the *GUS* gene. There will be a “scare” of 24 amino acids
 629 between *ALBA* and *GFP*. LB = left border, RB = right border, *HygroR* = *Hygromycin*
 630 resistance gene. The cartoon is not to scale. **(B)** *ALBA*-GFP expression in root tips.
 631 The GFP fluorescence was green; the nuclei were stained by DAPI, illuminating in
 632 blue; the bright field was under transmitted white light. Red arrows indicate the root
 633 cap and the epidermis. Scale bars = 40 μ m. **(C)** The GFP fluorescence; DAPI staining
 634 and bright field microscopy of *ALBA1-GFP*, *ALBA2-GFP*, *ALBA4-GFP*, *ALBA5-GFP*
 635 and *35S-GFP* root tips. Scale bars = 20 μ m.

636 **Figure 5. Characterization of the *alba4*, *alba5* and *alba6* mutants.** **(A)** The
 637 positions of the T-DNA insertion in the *alba4*, *alba5*, and *alba6* alleles. The *ALBA*
 638 genes are drawn to scale. **(B)** *ALBA* mRNA levels x-day old plants of Col-0 and
 639 *alba456*. Each measurement represents three biological replicate, with each replicate
 640 being composed of three individual plants. RNA levels were normalized to
 641 *CYCLOPHILIN*. The error bars represent the standard deviation of the means.

642 **Figure 6. Phenotypic analysis of Col-0, *alba456-1* and *alba456-2*.** **(A)** Rosette area
 643 from 14- to 26-days old plants. There was a significant difference of the rosette area
 644 development between the three groups ($p < 0.001$). **(B)** The curves of the rosette leaves
 645 number of *Col-0* and the mutants. There was no significance between them ($p > 0.05$).
 646 For **(A)** and **(B)**, the technical replicates are the measurements ($n=3$), the biological
 647 replicates are the plants of *Col-0* ($n=28$), *alba456-1* ($n=28$) and *alba456-2* ($n=29$).
 648 The grey shadow flanking the curve is the confidence interval; the significance of the
 649 differences was defined by the ANOVA and Tukey’s HSD following the linear mixed
 650 model. **(C)** The flowering-time of *Col-0*, *alba456-1*, and *alba456-2*. Aerial view of
 651 26-days old plants of the different genotypes. Red arrows indicate flowers. **(D)** The
 652 boxplot of the flowering-time. The biological replicates were individual plants in each
 653 group (*Col-0*: $n=28$, *alba456-1*: $n=28$, *alba456-2*: $n=29$). The centerline in the box is
 654 the median; the box indicates where the middle 50% of the data lie; the “whiskers”

655 indicate a "reasonable" estimate of the spread of the data. The *alba456-1* and
 656 *alba456-2* possessed a significantly later flowering-time than *Col-0*. However, there is
 657 no significant difference between *alba456-1* and *alba456-2* (**** denotes $p < 0.0001$,
 658 "ns" indicates "no significant difference", analyzed by Student's t-test).

659 **Figure 7. A delayed flowering-time segregates with the *alba456* genotype.**

660 Flowering-time were scored from progenies derived from either an
 661 *ALBA4/alba4-alba56* ($n=27$) or *alba45-ALBA6/alba6* ($n=27$) parents, as well as *Col-0*
 662 ($n=4$), all of which were grown under identical conditions. Compared to *Col-0*, the
 663 flowering-time of *ALBA4-alba56* was not significantly different,
 664 *ALBA4/alba4-alba56* had slightly delayed flowering ($p < 0.05$), *alba45-ALBA6* and
 665 *alba45-ALBA6/alba6* exhibited a more significant delayed flowering ($p < 0.01$),
 666 whereas the *alba456* had strongly delayed flowering ($p < 0.0001$). The "ns" denotes no
 667 significant difference, * denotes $p < 0.05$, ** denotes $p < 0.01$, **** denotes $p < 0.0001$
 668 (Student's t-test).

669 **Figure 8. The MA plot of all identified genes in *Col-0* and *alba456*.** The x-axis

670 represents value A (log2 transformed mean expression level). The y-axis represents
 671 value M (log2 transformed fold change in *alba456* compared to *Col-0*). Red dots
 672 represent up-regulated DEGs ($M \geq 1$). Blue dots represent down-regulated DEGs
 673 ($M \leq 1$). Gray points represent non-DEGs.

674 **Supplementary Figure Legends**

675 **Figure S1. Phylogenetic alignment of ALBA proteins from divergent species**

676 **across the plant kingdom.** A. *thaliana* proteins highlighted in green and identified by
 677 the code 'At.ALBA'. The proteins from other species are identified by the code at the
 678 start of the gene ID. This includes *Oryza sativa*: 'LOC_Os', *Sorghum bicolor*:
 679 'Sobic.', *Populus trichocarpa*: 'Potri.', *Medicago truncatula*: 'Medtr', *Mimulus*
 680 *guttatus*: 'Migut.', *Amborella trichopoda*: 'AmTr_v1.0_scaffold', *Physcomitrella*

681 *patens*: ‘Pp’, and *Chlamydomonas reinhardtii*: ‘Cre’. ALBA proteins across the plant
682 kingdom fall into two families with members of both families present in all
683 organisms. Clade A share a characteristic NEIRIT motif at the start of the Alba
684 domain. Clade B shares a characteristic NRIQVS motif at the start of the Alba
685 domain. Node values are ultrafast bootstrap support percentages.

686 **Figure S2. The amplicons of *attB*-ALBA sequences.** The 5` intergenic region
687 contained the genomic sequence from the stop codon of the upstream gene to the start
688 codon of the *ALBA* gene. The *ALBA* gene sequences contained all the exons and
689 introns except the stop codon, and no 3` intergenic sequences were included. The
690 *attB1* and *attB2* sites were incorporated to make the amplicon compatible for Gateway
691 cloning. The lengths of the amplicons are indicated in base pairs.

692 **Figure S3. GUS staining in leaves and reproductive organs of *ALBA*-GUS**
693 **transgenic plants.** (A) GUS staining of leaves of *ALBA*-GUS plants. (B) GUS
694 staining of mature flowers and siliques of *ALBA*-GUS plants. Each picture is a
695 representative of least three independent primary transformants examined. Scale bars
696 = 1 mm.

697 **Figure S4. ALBA4-GFP and ALBA5-GFP localization in leaf mesophyll cells.**
698 GFP fluorescence (green) and chlorophyll fluorescence (red) in leaf mesophyll cells.
699 Scale bars = 20 µm.

700 **Figure S5. Germination kinetics of Col-0, *alba123-1* and *alba123-2*.** Germination
701 (radicle emergence) was scored for Col-0 (*n* = 142), *alba123-1* (*n* = 173) and
702 *alba123-2* (*n* = 155), distributed over three different plates for each genotype.

703 **Figure S6. An independent replicate of rosette growth and flowering-time of**
704 **Col-0, *alba123-1* and *alba123-2*.** Col-0 (*n* = 29), *alba123-1* (*n* = 28) and *alba123-2*
705 (*n* = 29) were grown side-by-side as shown in Figure 7C. (A) The rosette area of the
706 three genotypes from 16- to 26-days old. (B) The flowering-time of the three

707 genotypes. (**** denotes $p < 0.0001$, “ns” indicates “no significant difference”,
708 Student’s t-test).

709 **Figure S7. Rosette growth and flowering-time of Col-0, *alba123-1* and *alba123-2***
710 **under short-day condition.** Col-0 ($n = 29$), *alba123-1* ($n = 19$) and *alba123-2*, ($n = 20$)
711 were grown under identical conditions to the long-day condition experiment except that
712 the photoperiod was only 10 hours per day. (A) Rosette area from 20- to 34-days old
713 plants. The area of Col-0 increased significantly faster than that of *alba123-1* and
714 *alba123-2* ($p < 0.001$, linear mixed model, ANOVA and Tukey’s HSD). (B) The
715 flowering-time of Col-0, *alba123-1* and *alba123-2* under short-day conditions. The
716 plant was scored as flowering when the bolting shoot reached 1 cm. **** indicates
717 $p < 0.001$, “ns” indicates no significance (Student’s t-test).

718 **Figure S8. The different alternative splicing events and their percentages in Col-0**
719 **and *alba123*.** The x-axis denotes the samples, the y-axis denotes the percentage. The
720 colors denote the particular splicing event (MXE denotes the Mutually exclusive exons,
721 AS5S denotes the Alternative 5' Splicing Site, RI denotes the Retained Intron, SE
722 denotes Skipped Exon and A3SS denotes Alternative 3' Splicing Site).

723 **Figure S9. The GO enrichment analysis and KEGG pathway enrichment analysis.**
724 (A) The GO enrichment with biological process ontology. The Y-axis is the number of
725 DEGs, the X-axis is the annotated GO terms. (B) The KEGG pathway enrichment
726 analysis. The Y-axis is the number of DEGs, the X-axis is the annotated pathways. The
727 pathways related to metabolism were outlined in red.

References

- Alonso JM, Stepanova AN, Leisse TJ, *et al.*** 2003. Genome-wide insertional mutagenesis of *Arabidopsis thaliana*. *Science* **301**, 653-657.
- Alvarez JP, Furumizu C, Efroni I, Eshed Y, Bowman JL.** 2016. Active suppression of a leaf meristem orchestrates determinate leaf growth. *Elife* **5**, e15023.
- Bell SD, Botting CH, Wardleworth BN, Jackson SP, White MF.** 2002. The interaction of Alba, a conserved archaeal chromatin protein, with Sir2 and its regulation by acetylation. *Science* **296**, 148-151.
- Boyes DC, Zayed AM, Ascenzi R, Mccaskill AJ, Hoffman NE, Davis KR, Gorlach J.** 2001. Growth stage-based phenotypic analysis of *Arabidopsis*: a model for high throughput functional genomics in plants. *The Plant Cell* **13**, 1499-1510.
- Chan CW, Kiesel BR, Mondragon, A.** 2018. Crystal Structure of Human Rpp20/Rpp25 Reveals Quaternary Level Adaptation of the Alba Scaffold as Structural Basis for Single-stranded RNA Binding. *Journal of Molecular Biology* **430**, 1403-1416.
- Chazotte B.** 2011. Labeling nuclear DNA using DAPI. *Cold Spring Harb Protocols* 2011, pdb prot5556.
- Chene A, Vembar SS, Riviere L, Lopez-Rubio J J, Claes A, Siegel TN, Sakamoto H, Scheidig-Benatar C, Hernandez-Rivas R, Scherf A.** 2012. PfAlbas constitute a new eukaryotic DNA/RNA-binding protein family in malaria parasites. *Nucleic Acids Resarch* **40**, 3066-3077.
- Cho H, Cho HS, Hwang I.** 2019. Emerging roles of RNA-binding proteins in plant development. *Current Opinion in Plant Biology* **51**, 51-57.
- Clough SJ, Bent AF.** 1998. Floral dip: a simplified method for *Agrobacterium*-mediated transformation of *Arabidopsis thaliana*. *The Plant Journal* **16**, 735-743.

- Curtis MD, Grossniklaus U.** 2003. A gateway cloning vector set for high-throughput functional analysis of genes in planta. *Plant Physiology* **133**, 462-469.
- Da Costa KS, Galucio JMP, Leonardo ES, Cardoso G, Leal E, Conde G, Lameira J.** 2017. Structural and evolutionary analysis of Leishmania Alba proteins. *Molecular and Biochemical Parasitology* **217**, 23-31.
- Dupe A, Dumas C, Papadopoulou B.** 2014. An Alba-domain protein contributes to the stage-regulated stability of amastin transcripts in Leishmania. *Molecular Microbiology* **91**, 548-561.
- Dupe A, Dumas C, Papadopoulou B.** 2015. Differential Subcellular Localization of Leishmania Alba-Domain Proteins throughout the Parasite Development. *PLoS One* **10**, e0137243.
- Edwards K, Johnstone C, Thompson C.** 1991. A simple and rapid method for the preparation of plant genomic DNA for PCR analysis. *Nucleic Acids Research* **19**, 1349
- Goodstein DM, Shu S, Howson R, et al.** 2012. Phytozome: a comparative platform for green plant genomics. *Nucleic Acids Research* **40**, D1178-1186
- Gosai SJ, Foley SW, Wang D, Silverman IM, Selamoglu N, Nelson AD, Beilstein MA, Daldal F, Deal RB, Gregory BD.** 2015. Global analysis of the RNA-protein interaction and RNA secondary structure landscapes of the Arabidopsis nucleus. *Molecular Cell* **57**, 376-388.
- Goyal M, Banerjee C, Nag S, Bandyopadhyay U.** 2016. The Alba protein family: Structure and function. *Biochimica et Biophysica Acta* **1864**, 570-583.
- Grillet L, Lan P, Li W, Mokkapati G, Schmidt W.** 2018. IRON MAN is a ubiquitous family of peptides that control iron transport in plants. *Nature Plants* **4**, 953-963.
- Guo L, Ding J, Guo R, Hou Y, Wang D-C, Huang L.** 2014. Biochemical and structural insights into RNA binding by Ssh10b, a member of the highly

conserved Sac10b protein family in Archaea. *The Journal of Biological Chemistry* **289**, 1478-1490.

Guo R, Xue H, Huang L. 2003. Ssh10b, a conserved thermophilic archaeal protein, binds RNA in vivo. *Molecular Microbiology* **50**, 1605-1615.

Hands-Taylor KL, Martino L, Tata R, Babon JJ, Bui TT, Drake AF, Beavil RL, Pruijn GJ, Brown PR, Conte MR. 2010. Heterodimerization of the human RNase P/MRP subunits Rpp20 and Rpp25 is a prerequisite for interaction with the P3 arm of RNase MRP RNA. *Nucleic Acids Research* **38**, 4052-4066.

Hentze MW, Castello A, Schwarzl T, Preiss T. 2018. A brave new world of RNA-binding proteins. *Nature Reviews Molecular Cell Biology* **19**, 327-341.

Honkanen S, Jones VAS, Morieri G, Champion C, Hetherington AJ, Kelly S, Proust H, Saint-Marcoux D, Prescott H, Dolan L. 2016. The Mechanism Forming the Cell Surface of Tip-Growing Rooting Cells Is Conserved among Land Plants. *Current Biology* **26**, 3238-3244.

Hothorn T, Bretz F, Westfall P. 2008. Simultaneous inference in general parametric models. *Biometrical Journal* **50**, 346-363.

Jelinska C, Conroy MJ, Craven CJ, Hounslow AM, Bullough PA, Waltho JP, Taylor GL, White MF. 2005. Obligate heterodimerization of the archaeal Alba2 protein with Alba1 provides a mechanism for control of DNA packaging. *Structure* **13**, 963-971.

Laurens N, Driessen RPC, Heller I, Vorselen D, Noom MC, Hol FJH, White MF, Dame RT, Wuite GJL. 2012. Alba shapes the archaeal genome using a delicate balance of bridging and stiffening the DNA. *Nature Communications* **3**, 1328.

Lewandowska M, Wawrzynska A, Moniuszko G, et al. 2010. A contribution to identification of novel regulators of plant response to sulfur deficiency: characteristics of a tobacco gene UP9C, its protein product and the effects of UP9C silencing. *Molecular Plant* **3**, 347-360.

- Madej T, Lanczycki C J, Zhang D, Thiessen PA, Geer RC, Marchler-Bauer A, Bryant SH.** 2014. MMDB and VAST+: tracking structural similarities between macromolecular complexes. *Nucleic Acids Research* **42**, D297-303.
- Mani J, Guttinger A, Schimanski B, Heller M, Acosta-Serrano A, Pescher P, Spath G, Roditi I.** 2011. Alba-domain proteins of *Trypanosoma brucei* are cytoplasmic RNA-binding proteins that interact with the translation machinery. *PLoS One* **6**, e22463.
- Marondedze C, Thomas L, Serrano NL, Lilley KS, Gehring C.** 2016. The RNA-binding protein repertoire of *Arabidopsis thaliana*. *Scientific Reports* **6**, 29766.
- Ozdilek BA, Thompson VF, Ahmed NS, White CI, Batey RT, Schwartz JC.** 2017. Intrinsically disordered RGG/RG domains mediate degenerate specificity in RNA binding. *Nucleic Acids Research* **45**, 7984-7996.
- Palm D, Simm S, Darm K, Weis BL, Ruprecht M, Schleiff E, Scharf C.** 2016. Proteome distribution between nucleoplasm and nucleolus and its relation to ribosome biogenesis in *Arabidopsis thaliana*. *RNA Biology* **13**, 441-454.
- Patterson K, Walters LA, Cooper AM, Olvera JG, Rosas MA, Rasmusson AG, Escobar MA.** 2016. Nitrate-Regulated Glutaredoxins Control *Arabidopsis* Primary Root Growth. *Plant Physiology* **170**, 989-999.
- Perez-Diaz L, Silva TC, Teixeira SMR.** 2017. Involvement of an RNA binding protein containing Alba domain in the stage-specific regulation of beta-amastin expression in *Trypanosoma cruzi*. *Molecular and Biochemical Parasitology* **211**, 1-8.
- Reichel M, Liao Y, Rettel M, Ragan C, Evers M, Alleaume AM, Horos R, Hentze MW, Preiss T, Millar AA.** 2016. In Planta Determination of the mRNA-Binding Proteome of *Arabidopsis* Etiolated Seedlings. *The Plant Cell* **28**, 2435-2452.
- Reiner R, Alfiya-Mor N, Berrebi-Demma M, Wesolowski D, Altman S, Jarrous N.** 2011. RNA binding properties of conserved protein subunits of human

RNase P. Nucleic Acids Research **39**, 5704-5714.

Silverman IM, Li F, Gregory BD. 2013. Genomic era analyses of RNA secondary structure and RNA-binding proteins reveal their significance to post-transcriptional regulation in plants. Plant Science **205-206**, 55-62.

Steffen A, Elgner M, Staiger D. 2019. Regulation of flowering time by the RNA-binding proteins AtGRP7 And AtGRP8. Plant Cell Physiol. Jun 26. pii: pcz124.

Subota I, Rotureau B, Blisnick T, Ngwabyt S, Durand-Dubief M, Engstler M, Bastin P. 2011. ALBA proteins are stage regulated during trypanosome development in the tsetse fly and participate in differentiation. Molecular Biology of the Cell **22**, 4205-4219.

Szostak E, Gebauer F. 2013. Translational control by 3'-UTR-binding proteins. Briefings in Functional Genomics **12**, 58-65.

Tanaka T, Padavattan S, Kumarevel T. 2012. Crystal structure of archaeal chromatin protein Alba2-double-stranded DNA complex from Aeropyrum pernix K1. The Journal of Biological Chemistry **287**, 10394-10402.

Torti S, Fornara F, Vincent C, Andres F, Nordstrom K, Gobel U, Knoll D, Schoof H, Coupland G. 2012. Analysis of the Arabidopsis shoot meristem transcriptome during floral transition identifies distinct regulatory patterns and a leucine-rich repeat protein that promotes flowering. The Plant Cell **24**, 444-462.

Vasilyev N, Polonskaia A, Darnell JC, Darnell RB, Patel DJ, Serganov A. 2015. Crystal structure reveals specific recognition of a G-quadruplex RNA by a beta-turn in the RGG motif of FMRP. Proceedings of the National Academy of Science USA **112**, E5391-E5400.

Verma JK, Gayali S, Dass S, Kumar A, Parveen S, Chakraborty S, Chakraborty N. 2014. *OsAlba1*, a dehydration-responsive nuclear protein of rice (*Oryza sativa* L. ssp. indica), participates in stress adaptation. Phytochemistry **100**, 16-25.

- Verma JK, Wardhan V, Singh D, Chakraborty S, Chakraborty N.** 2018. Genome-wide identification of the Alba gene family in plants and stress-responsive expression of the rice Alba genes. *Genes (Basel)* **9**, 183
- Wardleworth BN, Russell RJ, Bell SD, Taylor GL, White MF.** 2002. Structure of Alba: an archaeal chromatin protein modulated by acetylation. *EMBO Journal* **21**, 4654-4662.
- Wickham H.** 2016. *ggplot2: Elegant Graphics for Data Analysis*, New York, Springer-Verlag.
- Wu J, Niu S, Tan M, et al.** 2018. Cryo-EM Structure of the Human Ribonuclease P Holoenzyme. *Cell* **175**, 1393-1404 e11.
- Wu Z, Zhu D, Lin X, et al.** 2016. RNA Binding Proteins RZ-1B and RZ-1C Play Critical Roles in Regulating Pre-mRNA Splicing and Gene Expression during Development in Arabidopsis. *The Plant Cell* **28**, 55-73.
- Yuan W, Zhou J, Tong J, Zhuo W, Wang L, Li Y, Sun Q, Qian W.** 2019. ALBA protein complex reads genic R-loops to maintain genome stability in *Arabidopsis*. *Scientific Advances* **5**, eaav9040.
- Zhang Z, Boonen K, Ferrari P, Schoofs L, Janssens E, van Noort V, Rolland F, Geuten K.** 2016 UV crosslinked mRNA-binding proteins captured from leaf mesophyll protoplasts. *Plant Methods* **12**, 42.
- Zuo Y, Feng F, Qi W, Song R.** 2019. Dek42 encodes an RNA binding protein that affects alternative pre-mRNA splicing and maize kernel development. *Journal of Integrative Plant Biology* **61**, 728-748.

Figure 1

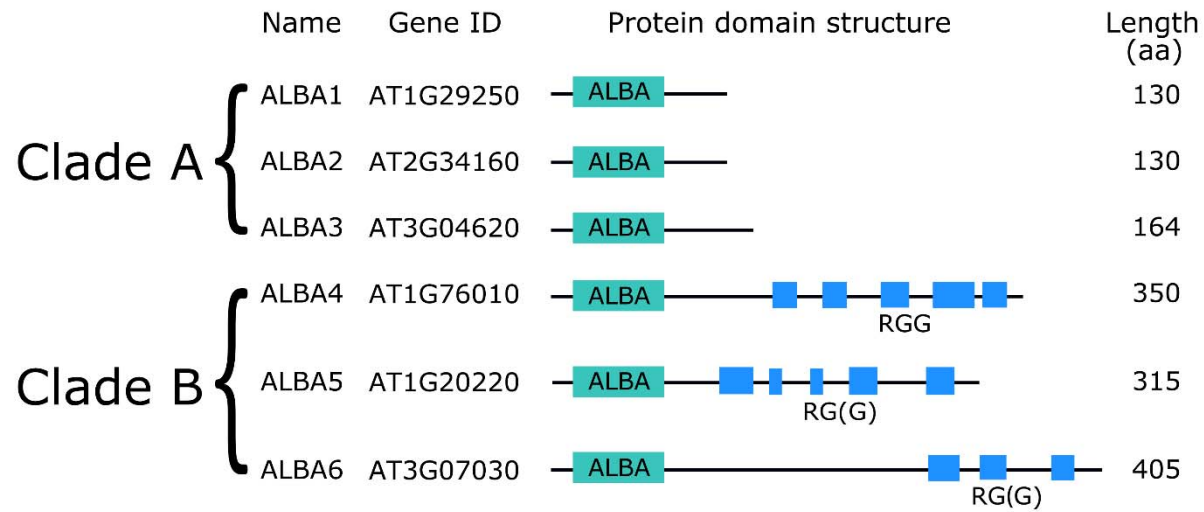


Figure 1. The Arabidopsis ALBA proteins. AT number, domain structure and amino acid length are shown for each gene.

Figure 2

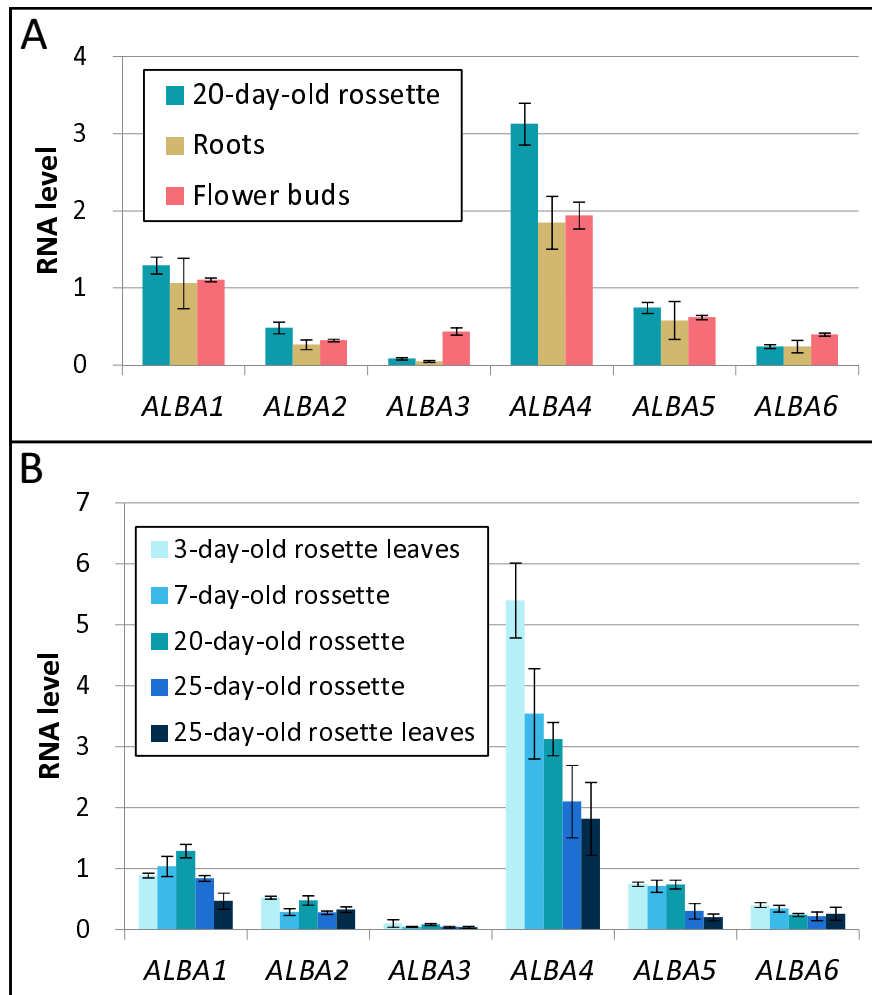


Figure 2. qRT-PCR transcript profiling of the six *ALBA* genes in *Arabidopsis*. (A) mRNA levels in root, rosettes and flowers. (B) mRNA levels at different stages of rosette growth. All levels are normalized to *CYCLOPHILIN*. All measurements are the mean of three biological replicates, each of which was determined by three technical replicates ($n=3$). The error bars are the standard deviations.

Figure 3

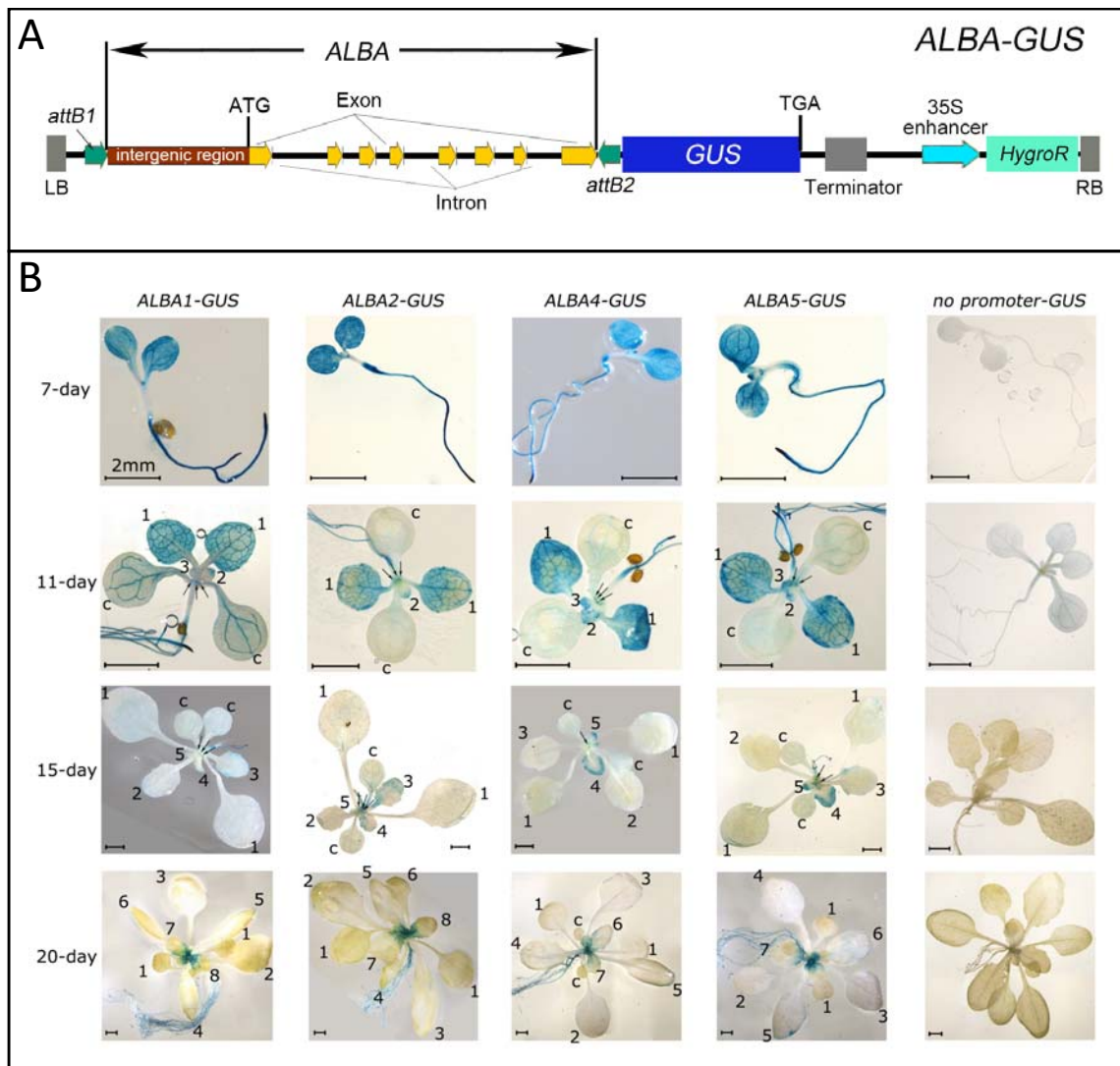


Figure 3 The expression of *ALBA-GUS* transgenes during vegetative development. (A) Schematic representation of the *ALBA-GUS* translational fusion for *ALBA1*, *ALBA2*, *ALBA4*, and *ALBA5* in the pMDC163 vector. DNA sequences contain 5' intergenic regions, exon and intron region up, but not including the stop codon, were cloned in frame with the *GUS* gene. There will be a "scare" of 28 amino acids between the *ALBA* and *GUS*. LB = left border, RB = right border, *HygroR* = *Hygromycin* resistance gene. The cartoon is not to scale. **(B)** Expression patterns of *ALBA1-GUS*, *ALBA2-GUS*, *ALBA4-GUS*, *ALBA5-GUS* and *pMDC164* transgenic *Arabidopsis* throughout vegetative development (7-, 11-, 15- and 20-day old plants are presented). Each picture is representative of at least three independent primary transformants analysed. The order of the leaf emergence is labeled ("c" denotes cotyledon, "1" denotes the first pair of leaves, "2" denotes the second leaf, etc). The vegetative meristem in the shoot apex region is indicated with black arrows. Scale bars = 2 mm.

Figure 4

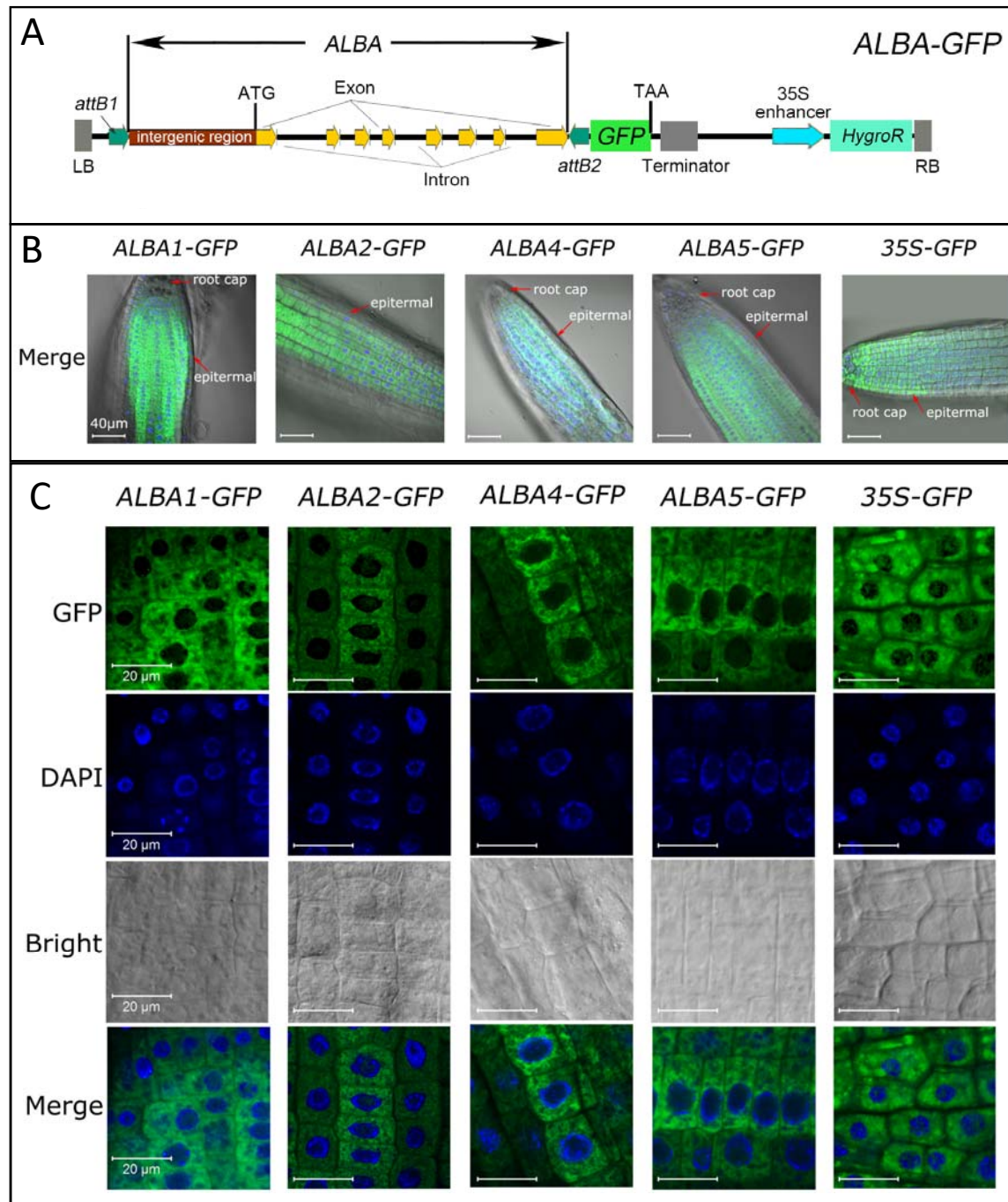


Figure 4. The subcellular localization of the ALBA proteins. (A) Schematic representation of the *ALBA-GFP* translational fusion for *ALBA1*, *ALBA2*, *ALBA4*, and *ALBA5* in the pMDC111 vector. DNA sequences contain 5' intergenic regions, exon and intron region up, but not including the stop codon, were cloned in frame with the *GUS* gene. There will be a "scar" of 24 amino acids between *ALBA* and *GFP*. LB = left border, RB = right border, *HygroR* = *Hygromycin* resistance gene. The cartoon is not to scale. **(B)** *ALBA-GFP* expression in root tips. The GFP fluorescence was green; the nuclei were stained by DAPI, illuminating in blue; the bright field was under transmitted white light. The root cap and the epidermis are indicated with red arrows. Scale bars = 40 μ m. **(C)** The GFP fluorescence; DAPI staining and bright field microscopy of *ALBA1-GFP*, *ALBA2-GFP*, *ALBA4-GFP*, *ALBA5-GFP* and *35S-GFP* root tips. Scale bars = 20 μ m.

Figure 5

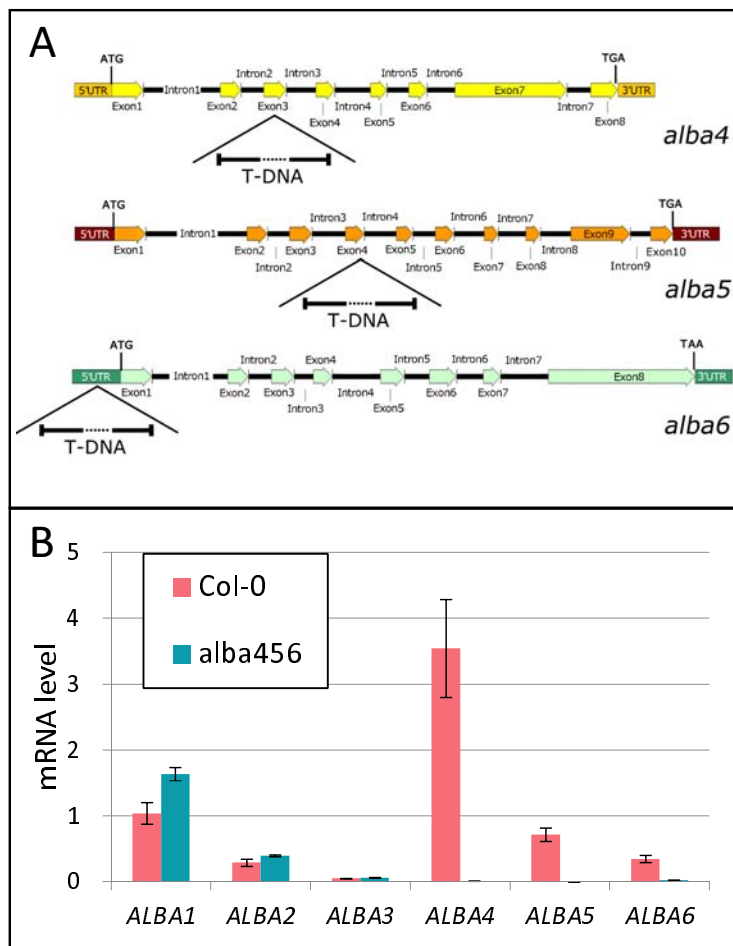


Figure 5. Characterization of the *alba4*, *alba5* and *alba6* mutants. (A) The positions of the T-DNA insertion in the *alba4*, *alba5*, and *alba6* alleles. The *ALBA* genes are drawn to scale. **(B)** *ALBA* mRNA levels x-day old plants of Col-0 and *alba456*. Each measurement represents three biological replicate, with each replicate being composed of three individual plants. RNA levels were normalized to *CYCLOPHILIN*. The error bars represent the standard deviation of the means.

Figure 6

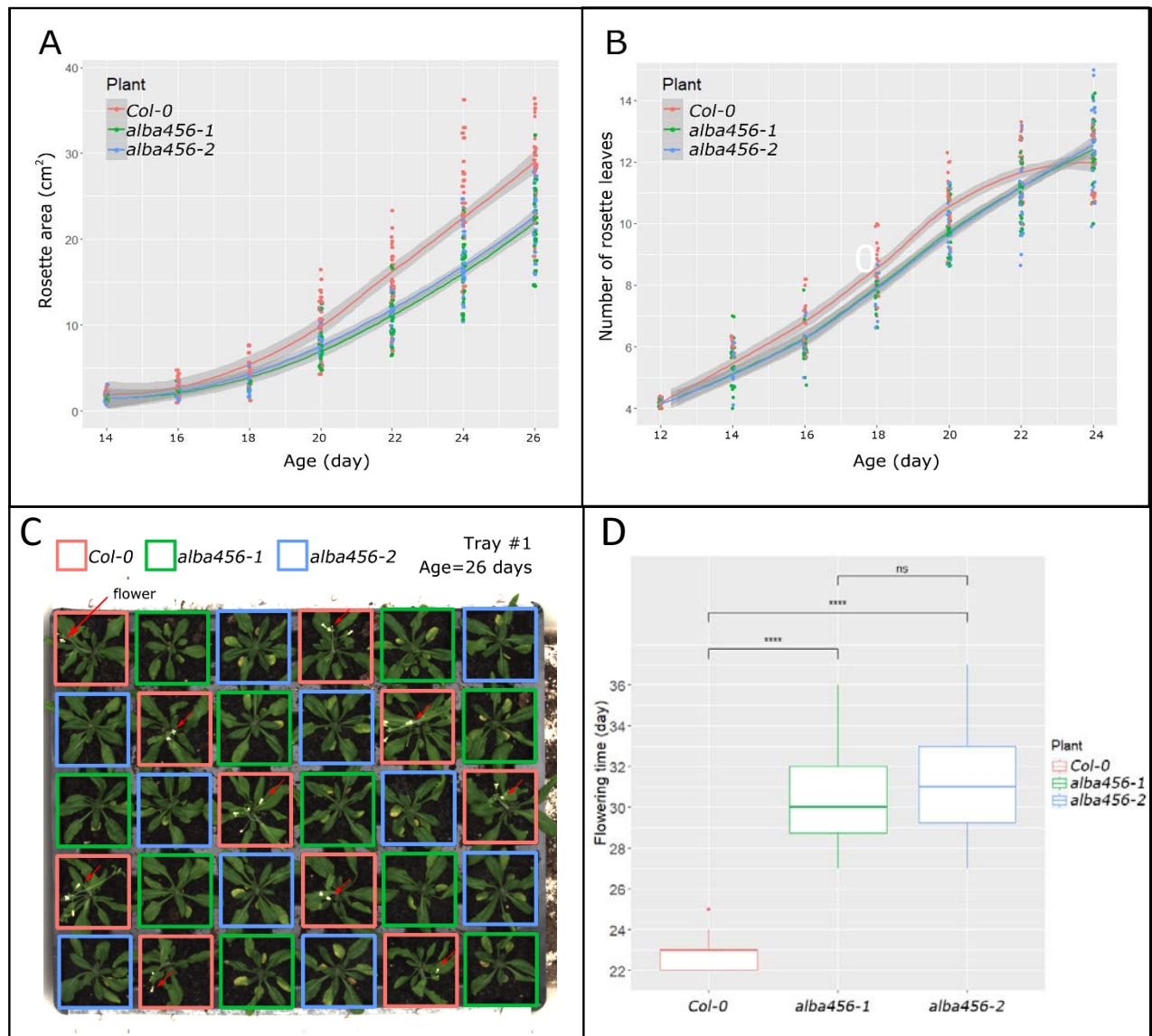


Figure 6. Phenotypic analysis of *Col-0*, *alba456-1* and *alba456-2*. (A) Rosette area from 14- to 26-days old plants. There was a significant difference of the rosette area development between the three groups ($p < 0.001$). (B) The curves of the rosette leaves number of *Col-0* and the mutants. There was no significance between them ($p > 0.05$). For (A) and (B), the technical replicates are the measurements ($n = 3$), the biological replicates are the plants of *Col-0* ($n = 28$), *alba456-1* ($n = 28$) and *alba456-2* ($n = 29$). The grey shadow flanking the curve is the confidence interval; the significance of the differences was defined by the ANOVA and Tukey's HDS following the linear mixed model. (C) The flowering-time of *Col-0*, *alba456-1*, and *alba456-2*. Aerial view of 26-days old plants of the different genotypes. Red arrows indicate flowers. (D) The boxplot of the flowering-time. The biological replicates were individual plants in each group (*Col-0*: $n = 28$, *alba456-1*: $n = 28$, *alba456-2*: $n = 29$). The centerline in the box is the median; the box indicates where the middle 50% of the data lie; the "whiskers" indicate a "reasonable" estimate of the spread of the data. The *alba456-1* and *alba456-2* possessed a significantly later flowering-time than *Col-0*. However, there is no significant difference between *alba456-1* and *alba456-2* (**** denotes $p < 0.0001$, "ns" indicates "no significant difference", analyzed by Student's t-test).

Figure 7

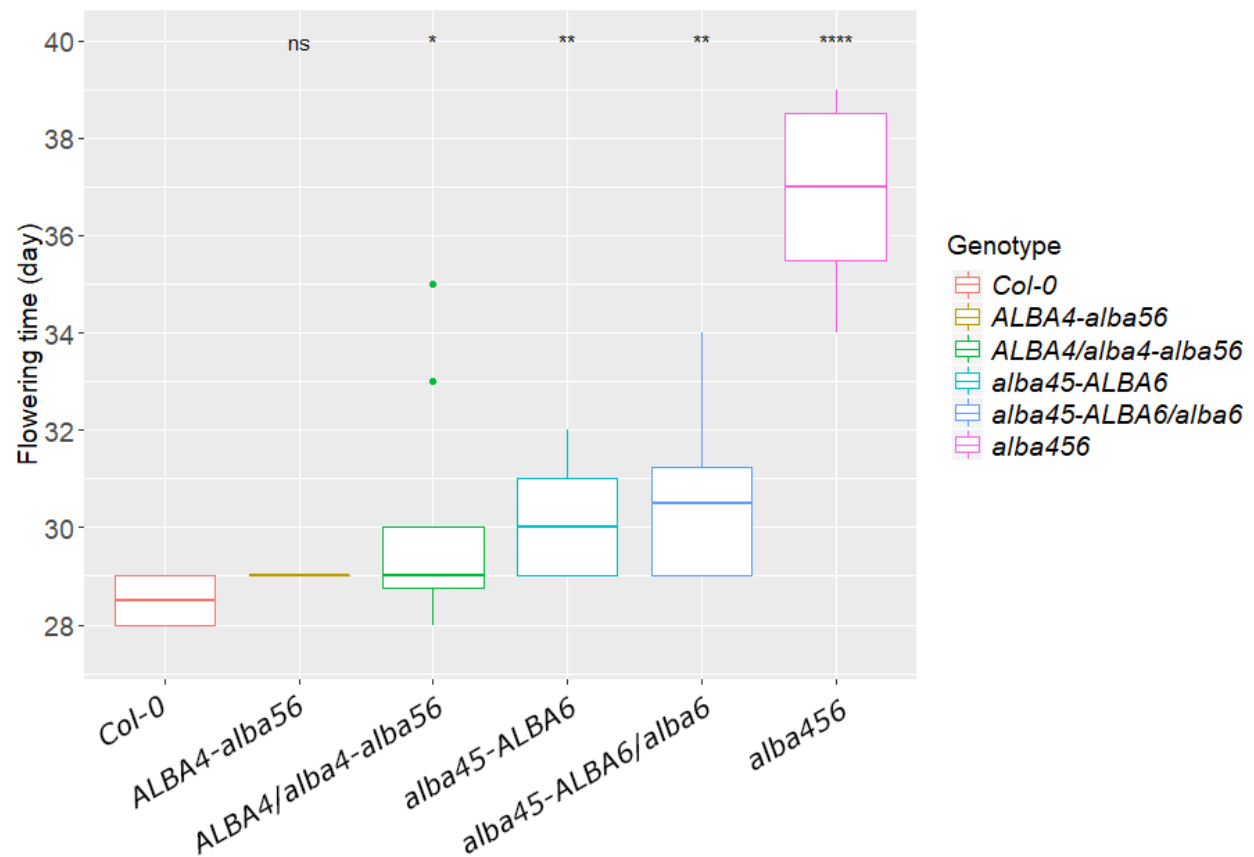


Figure 7. A delayed flowering-time segregates with the *alba456* genotype. Flowering-time were scored from progenies derived from either an *ALBA4/alba4-alba56* ($n=27$) or *alba45-ALBA6/alba6* ($n=28$) parents, as well as *Col-0* ($n=4$), all of which were grown under identical conditions. Compared to *Col-0*, the flowering-time of *ALBA4-alba56* was not significantly different, *ALBA4/alba4-alba56* had slightly delayed flowering ($p<0.05$), *alba45-ALBA6* and *alba45-ALBA6/alba6* exhibited a more significant delayed flowering ($p<0.01$), whereas the *alba456* had strongly delayed flowering ($p<0.0001$). The “ns” denotes no significant difference, * denotes $p<0.05$, ** denotes $p<0.01$, **** denotes $p<0.0001$ (Student’s t-test).

Figure 8

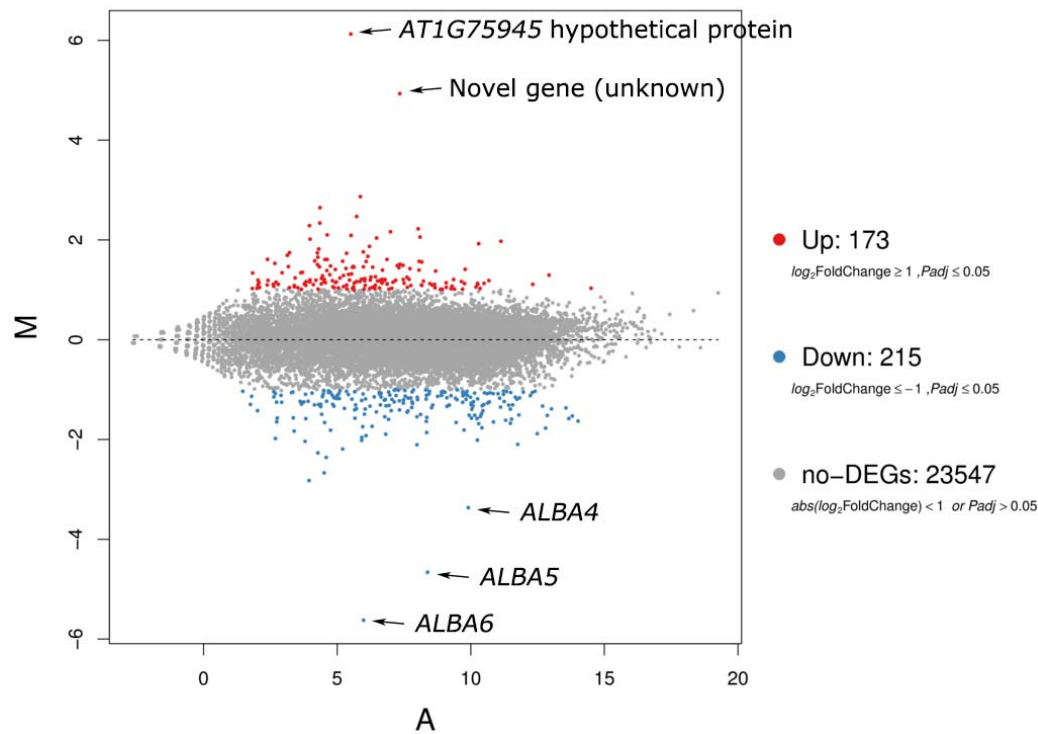


Figure 8. The MA plot of all identified genes in Col-0 and *alba456*. The x-axis represents value A (log2 transformed mean expression level). The y-axis represents value M (log2 transformed fold change in *alba456* compared to Col-0). Red dots represent up-regulated DEGs ($M \geq 1$). Blue dots represent down-regulated DEGs ($M \leq -1$). Gray points represent non-DEGs.